Two-color modulation transfer spectroscopy[1]

A. Pérez Galván, D. Sheng, L.A. Orozco, and Y. Zhao

Abstract: We present two-color modulation transfer spectroscopy as a tool for precision studies of atomic properties of excited states. The bi-colored technique addresses a narrow set of velocity groups of a thermal atomic vapour using a two-step transition to "burn a hole" in the velocity distribution. The resulting spectrum presents sub-Doppler linewidths, good signal-to-noise ratio and the trademark sidebands that work as an in situ ruler for the energy spacing between atomic resonances. The spectra obtained can be used for different applications such as measurements of energy splittings or stabilization of laser frequencies to excited atomic transitions.

PACS Nos.: 32.10.Fn, 32.30.−r, 42.50.Gy, 42.60.Fc

Résumé : Nous présentons la spectroscopie à transfert de modulation à deux couleurs comme un outil d'étude de précision des propriétés atomiques des états excités. Cette technique deux couleurs s'adresse à un ensemble étroit de groupes de vitesse d'une vapeur atomique therrmalisée en utilisant une transition en deux étapes pour « brûler un trou » dans la distribution de vitesse. Les spectres résultant présentent des largeurs de lignes sous-Doppler, un bon rapport signal sur bruit et des bandes latérales caractéristiques qui fonctionnent comme des standards *in situ* pour les séparations en énergie entre les résonances atomiques. Les spectres obtenus peuvent être utilisés pour différentes applications, comme des mesures de séparation en énergie ou de stabilisation de fréquence laser à des transitions atomiques excitées.

[Traduit par la Rédaction]

1. Introduction

Spectroscopic studies of hyperfine manifolds in alkalies, such as measurements of energy separations, have benefited from the high precision of the experimental techniques available to interrogate atoms [1]. The hydrogen-like structure of the atom makes interpretation of experimental results straightforward in terms of the electromagnetic fields generated by the valence electron and nuclear moments. Precise measurements in higher excited states accessible through two-step transitions [2–5] have appeared in recent years. This has renewed interest in improving calculations in other states where theoretical methods such as the many-body perturbation theory (MBPT) (see, for example, the recent book by Johnson [6]) are yet to be tested against experimental results.

Precise measurements in excited states, beyond the first one, have several experimental complications. Standard spectroscopic techniques rely on the high population of atoms in the ground state to guarantee a good signal-to-noise ratio of the fluorescence or absorption of the atomic sample. In two-step transitions this is no longer the case. The amount of population transferred to the intermediate level, for reasonable powers of the lasers, tends to be small, and detectors at the desired frequency might no be readily available.

We present, in this paper, two-color modulation transfer spectroscopy as a tool for studies of the atomic properties of higher excited states. The method consist of two lasers (pump and probe) counter-propagating through a thermal vapour. Before being directed to the interaction region, one of the lasers is modulated. The first step of the transition, i.e., the pump, connects the ground state to a resonant intermediate state while the probe scans over the desired energy manifold. We monitor the absorption of the pump laser as a function of the probe laser detuning. The nonlinear interaction of the lasers "burns a hole" in the atomic ground-state population. The generated spectra presents sub-Doppler peaks (sometimes called Lamb–Bennett dips) corresponding to the atomic resonances with the trademark sidebands at their side. This technique overcomes the two main inconveniences of direct absorption of the probing laser, i.e., a low signal-to-noise ratio and the nonavailability of detectors at the desired wavelength.

We present two ladder systems in ^{87}Rb to illustrate the main features of the technique and two different applications of the modulation. We select the $5S_{1/2} \rightarrow 5P_{1/2} \rightarrow 6S_{1/2}$ and the $5S_{1/2} \rightarrow 5P_{3/2} \rightarrow 5D_{5/2}$ ladder transitions to illustrate their different uses. The amplitude of the probe laser is modulated for the first system while the second system has its pump frequency modulated. The frequency modulation of the pump laser and a good signal-to-noise ratio allows us to lock the probe laser to the $5P_{3/2} \rightarrow 5D_{5/2}$ excited atomic resonance. In this case, the probe laser remains modulation free. This is highly desired since the electronic modulation of the laser itself can carry unwanted effects such as sidebands at higher or lower frequencies as well

Received 8 October 2008. Accepted 4 November 2008. Published on the NRC Research Press Web site at http://cjp.nrc.ca/ on 12 February 2009.

A. Pérez Galván, D. Sheng, and L.A. Orozco.[2] Joint Quantum Institute, Department of Physics, University of Maryland and National Institute of Standards and Technology, College Park, MD 20742-4100, USA.
Y. Zhao. State Key Laboratory of Quantum Optics and Quantum Optics Devices, College of Physics and Electronics Engineering, Shanxi University, Taiyuan 030006, China.

[1]This paper was presented at the Symposium on Atomic Physics: A tribute to Walter Johnson, held at the University of Notre Dame, Notre Dame, Indiana, USA, on 4–5 April 2008.
[2]Corresponding author (e-mail: lorozco@umd.edu).

 doi: 10.1139/P08-120

Fig. 1. Theoretical model of two-step transition with (*a*) amplitude-modulated probe and (*b*) frequency-modulated pump.

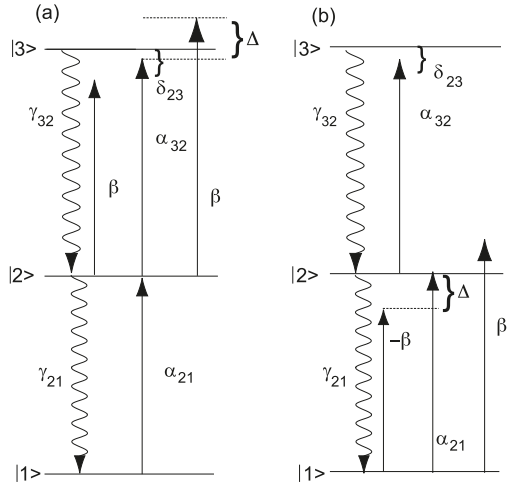

as bandwidth problems. The method we are presenting is, of course, not limited to these two cases and can be extended to other atomic levels.

The organization of the paper is as follows: Sect. 2 contains the theoretical model, Sect. 3 explains the experimental setup and results, Sect. 4 has a summary of the precise measurements using this method, and Sect. 5 presents the conclusions.

2. Theoretical model

We start with a three-level model that can show some of the qualitative features of the experimental spectra. We use a density matrix formalism to describe a three level atom in ladder configuration interacting with two lasers, one of which has sidebands. We model our system as Doppler-free ignoring Zeeman sublevels to keep it tractable. The experimental situation is more complex and for quantitative analysis it is necessary to take into account those same effects that we are ignoring.

Figure 1 shows our theoretical model. We treat two cases. Figure 1*a* is a ladder-type system with an amplitude-modulated probe (AMP). Figure 1*b* presents the same system except it has a frequency-modulated pump (FMP).

The intermediate and last levels are coupled by a single laser with three frequencies: a carrier and two sidebands separated from the carrier by Δ (in MHz). We represent the amplitude of the carrier by a Rabi frequency α_{32} and the sidebands by a modulation depth β. The ground and intermediate states are coupled by α_{21}. The detuning of the carrier between levels $|1\rangle$ and $|2\rangle$ is zero in the model as it is for our experiment and we let the detuning between levels $|2\rangle$ and $|3\rangle$ vary as δ_{23}. The total population is normalized to unity. Figure 1*b* follows the same nomenclature except that the sidebands arise from frequency modulation and they appear in the pump laser α_{21}. For the FMP systems the sidebands have the appropriate sign difference.

We have a set of nine linear equations for the slowly varying elements of the density matrix σ_{nm} after using the rotating wave approximation with the sidebands rotating — one clockwise, one counter clockwise — at a frequency Δ. The equations are

$$\sum_k (\gamma_{kn}\sigma_{kk} - \gamma_{nk}\sigma_{nn}) + \frac{i}{2}\sum_k (\alpha_{nk}\sigma_{kn} - \sigma_{nk}\alpha_{kn}) = \dot{\sigma}_{nm} \quad \text{for} \quad n = m$$

$$[i\,(\Omega_{nm} - \omega_{nm}) - \Gamma_{nm})]\,\sigma_{nm} + \frac{i}{2}\sum_k (\alpha_{nk}\sigma_{km} - \sigma_{nk}\alpha_{km}) = \dot{\sigma}_{nm} \quad \text{for} \quad n \neq m$$

where $\omega_{nm} = (E_n - E_m)/\hbar$ is the transition frequency, and $\Omega_{nm} = -\Omega_{mn}$ is the laser frequency connecting the levels. The damping rate is given by

$$\Gamma_{nm} = \frac{1}{2}\sum_k (\gamma_{nk} + \gamma_{mk})$$

and $\alpha_{21} = \alpha_{21}^0\left(1 + \beta e^{i\Delta t} - \beta e^{-i\Delta t}\right)$ for the FMP system and $\alpha_{32} = \alpha_{32}^0\left(1 + \beta e^{i\Delta t} + \beta e^{-i\Delta t}\right)$ for the AMP system. The time dependence of the Rabi frequency makes the standard approach of obtaining the steady-state solution of the system not feasible. Instead, we use a Floquet basis expansion of the density matrix [7] to solve our system of equations. We replace each of the slowly rotating elements of the density matrix by

$$\sigma_{nm}(t) = \sum_{k=-p}^{p} \sigma_{nm}^{(k)} e^{ik\Delta t}$$

where $\sigma_{nm}^{(k)}$ is the Fourier amplitude of the component oscillating at $k\Delta$. The system is now a series of $2p+1$ coupled equations for some large p that have to be solved recursively. It is necessary to set $\sigma_{nm}^{(p)} = 0$ for some p to cut off the infinite number of coupled equations. By solving the equations in terms of their predecessors we can extract $\sigma_{12}(t)$.

For our experiment, we are interested in the terms $\sigma_{12}^{(0)}$, $\sigma_{12}^{(-1)}$, and $\sigma_{12}^{(1)}$, which are proportional to the absorption of the first laser carrier and sidebands, respectively. We plot the absolute value of the imaginary part as a function of δ_{23} to recover the absorption. This is necessary to take into account the square-law nature of the photodiode. Our three level model reproduces the resonance features of the absorption observed as the second excitation goes into resonance for both the AMP and FMP systems (see Figs. 2 and 3, respectively). The demodulation of the FMP signal yields the expected error-like feature shown in Fig. 4.

The size of the sidebands in our model depends on the modulation index (separation from resonance and strength), as well as the specific decay rates of the levels that set up the Rabi frequencies α_{ij} in the AMP and FMP systems.

3. Apparatus and method

Figure 5 shows the specific energy levels in Rb used in the experiment, while Figs. 6 and 7 present block diagrams of the FMP and AMP systems, respectively. A Coherent 899-01 Ti:sapphire laser with a linewidth of less than 100 kHz is the pump laser in both cases. A small amount of laser power from the pump laser

Fig. 2. Numerical solution of the absorption of the pump laser as a function of the normalized detuning of the probe laser in units of γ_{21}. The parameters are (in units of γ_{21}): $\beta = 1/3$, $\alpha_{21} = 1/100$, $\alpha_{32}^0 = 1/4$, $\gamma_{32} = 1/2$, and $\Delta = 15$.

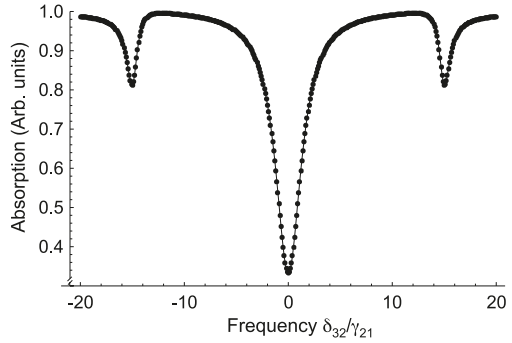

Fig. 3. Numerical solution of the absorption of the pump laser as a function of the normalized detuning of the probe laser in units of γ_{21}. The parameters are (in units of γ_{21}): $\beta = 1/10$, $\alpha_{12}^0 = 1/100$, $\alpha_{23} = 1/4$, $\gamma_{32} = 1/10$, and $\Delta = 2.5$.

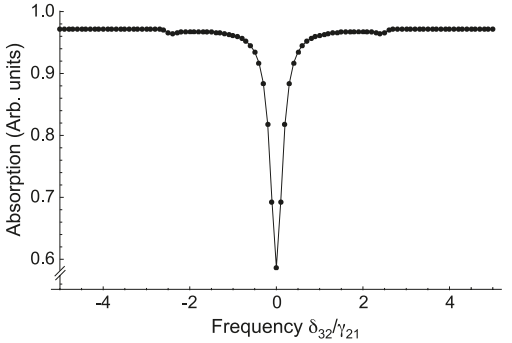

Fig. 4. Numerical simulation of the demodulated absorption of the pump laser for the FMP system as a function of the normalized detuning of the probe laser in units of γ_{21}. The parameters are (in units of γ_{21}): $\beta = 1/10$, $\alpha_{12}^0 = 1/100$, $\alpha_{32} = 1/4$, $\gamma = 1/10$, and $\Delta = 2.5$.

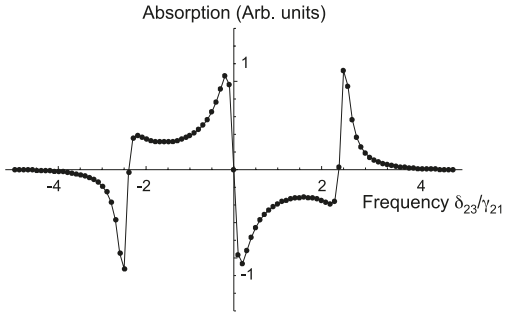

is frequency modulated by a small bandwidth electro-optical modulator at ≈15 MHz and sent to a glass cell filled with rubidium at room temperature to lock the laser frequency to the $5P_{3/2}$ crossover line of the $F = 1$ and $F = 3$ hyperfine levels for the FMP system and to the on resonance $F = 1 \rightarrow F = 2$ transition of the $5P_{1/2}$ level for the AMP system at 795 nm with a Pound–Drever–Hall lock.

Level $|1\rangle$ in the AMP system corresponds to the lower hyperfine state of the $5S_{1/2}$ level ($F = 1$) while $|2\rangle$ is the highest

Fig. 5. (*a*) Relevant energy levels for the modulation of the pump atomic system. (*b*) Relevant energy levels for the modulation of the probe atomic system.

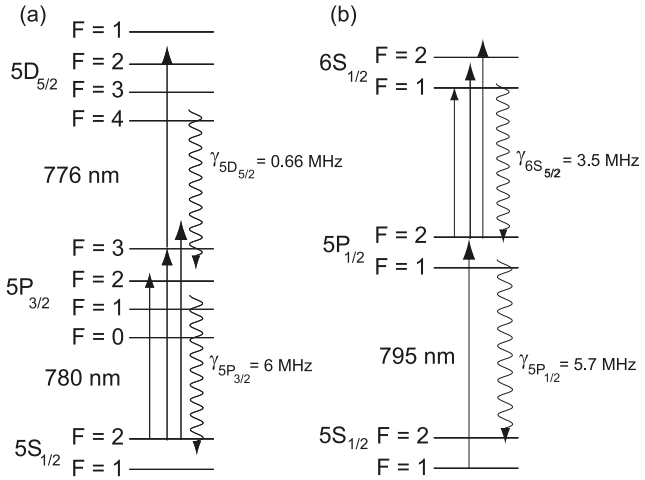

Fig. 6. Block diagram of the experiment. Key for the figure PD: photodiode, AOM: acousto-optical modulator, LO: local oscillator, BS: beam splitter.

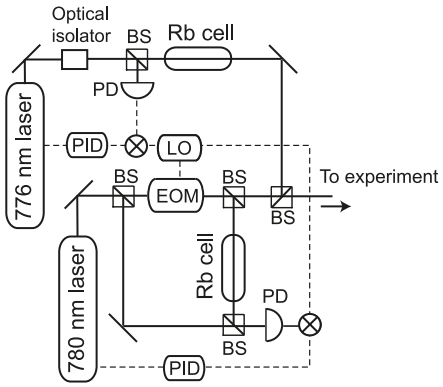

Fig. 7. Block diagram of the experiment. Key for the figure PD: photodiode, LO: local oscillator, BS: beam splitter.

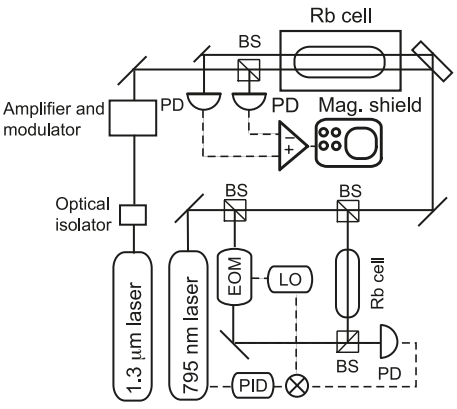

hyperfine state of the $5P_{1/2}$ level ($F = 2$) of ^{87}Rb. The decay rate between the two levels is $\gamma_{21}/2\pi = 5.7$ MHz [8]. We simplify the hyperfine states of the $6S_{1/2}$ level to just one level with decay rate $\gamma_{32}/2\pi = 3.5$ MHz [9].

For the FMP system, the probe laser is an SDL diode laser with a linewidth of 5 MHz at 776 nm. The lasers overlap in-

Fig. 8. Experimental trace for FMP showing the DC component of the absorption of the 780 nm laser as a function of the probe laser detuning as it scans across the $5D_{5/2}$ level in ^{87}Rb. It presents the main resonances as well as the indicated sidebands (SB). The power of the probe and pump beam are 4.3 mW and 100 μW, respectively.

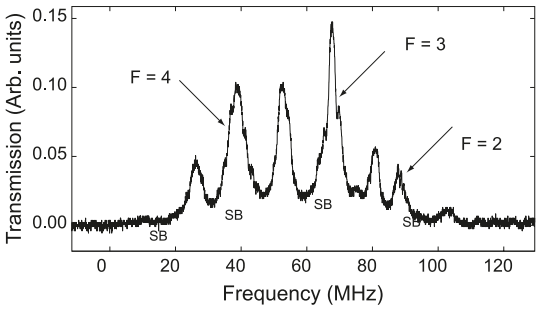

side an independent rubidium glass cell at room temperature wrapped in μ-metal in lin-perp-lin polarization configuration. Their $1/e^2$ power diameter of the laser beams is 1 mm. We scan the probe laser over the $5D_{5/2}$ level hyperfine manifold and observe the absorption of the pump laser as a function of the probe laser detuning using a fast photodetector. We send the signal to a bias-T and record the DC and demodulated AC components with a WaveSurfer digital oscilloscope with an 8-bit resolution from Lecroy.

We keep the power of the pump laser and the modulation depth fixed to a value of 100 μW and $\beta = 0.2$, respectively. We change the power of the probe beam and observe its influence on the spectra. It is possible to observe the resonant features of the $5D_{5/2}$ hyperfine manifold with as little as 100 μW of the probe power. Higher probe power increases the signal size and the width of the features. Playing with the polarization and powers, we also observe EIT features [10]. We restrict ourselves to a space parameter where these very narrow features are absent.

Figures 8 (FMP) and 9 (FMP) show typical experimental traces of the absorption of the 780 nm laser. The spectrum has been offset to zero transmission for convenience. The first of these, Fig. 8, has the DC component of the absorption with the sidebands appearing on both sides of the main resonances. No Doppler background is observed for any of the experimental conditions explored, showing that this is a Doppler-free spectrum. Figure 9*a* shows the lower hyperfine states of the $5D_{5/2}$ level manifold with no sidebands for clarity. Figure 9*b* has the demodulated AC component of the absorption. The broken lines identify the error-like features with their corresponding hyperfine levels. We use this spectrum to stabilize the frequency of the probe laser.

We monitor the laser frequency of the probe beam using a Coherent confocal Fabry–Perot cavity with a free spectral range of 1.5 GHz to test the performance of the laser lock. Figure 10 shows the fringe-side transmission of the probe laser through the cavity. We monitor the behavior of the laser before and after it has been locked. The reduction of the frequency excursions is quite evident as the laser is locked to the atomic resonance. Under normal experimental conditions we have observed locking times of 30 min, and a significant reduction of the rms noise by more than a factor of seven.

Fig. 9. Experimental traces for FMP for the $5D_{5/2}$ resonances in ^{87}Rb of (*a*) absorption without sidebands and (*b*) demodulated absorption of 780 nm laser as a function of detuning of the 776 nm laser. The power of the probe and pump beam are 4.3 mW and 100 μW, respectively.

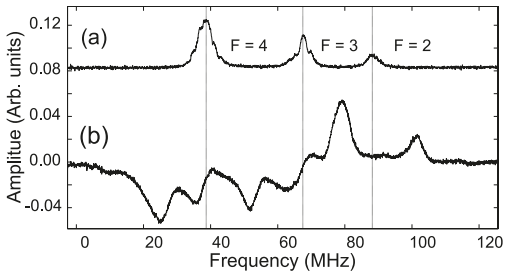

Fig. 10. Fringe-side transmission of the SDL laser at 776 nm through a confocal Fabry–Perot cavity. The reduction of the amplitude of the signal corresponds to the locking of the laser to the $5P_{3/2} \rightarrow 5D_{5/2}$ excited atomic transition using FMP.

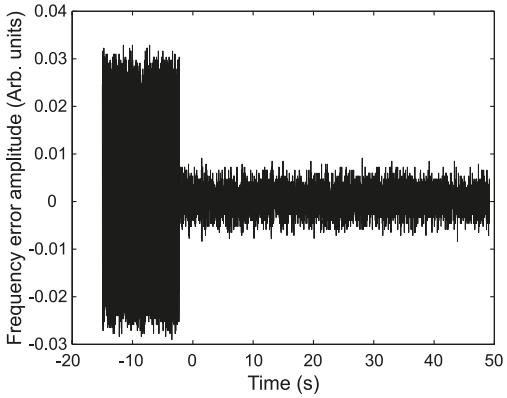

A thick glass plate splits the main beam at 795 nm into two in the AMP system before entering an independent rubidium-vapor glass cell inside a three-layered magnetic shield. A grating-narrowed diode laser at 1.324 μm (from here on referred to as a 1.3 μm laser) with a linewidth better than 500 kHz excites the second transition. We scan the frequency of the 1.3 μm laser over the hyperfine manifold of the $6S_{1/2}$ level. A fiber-coupled semiconductor amplifier increases the power of the 1.3 μm laser before it goes to a large bandwidth ($\approx$10 GHz) electro-optic modulator (EOM) that generates the sidebands.

The power of each 795 nm beam is approximately 10 μW with a diameter of 1 mm. We operate in the low-intensity regime to avoid power broadening, differential AC stark shifts, and line splitting effects such as the Autler–Townes splitting. Both beams are circularly polarized by a $\lambda/4$ waveplate. The counter-propagating 1.3 μm laser beam with a power of 4 mW and approximately equal diameter overlaps one of the 795 nm beams. After the glass cell, an independent photodiode detects each 795 nm beam. The outputs of the detectors go to a differential amplifier to reduce common noise. A digital oscilloscope records the output signal for different values of modulation. Figure 11 shows an absorption spectrum of the 795 nm laser as a function of the detuning of the 1.3 μm laser that shows the signature sidebands of the technique. Figure 12 shows a plot of the distance between the sidebands as a function of the

Fig. 11. Absorption profile of the $6S_{1/2}$, $F = 1$ and $F = 2$ hyperfine states of ^{87}Rb with sidebands. The big sideband belongs to the $F = 1$ peak. The small feature on the side of the $F = 2$ peak corresponds to the second sideband of the $F = 1$ peak. The glass cell is in a magnetic field of 0.37 G.

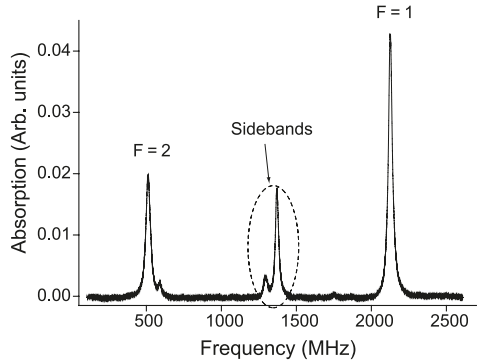

Fig. 12. Plot of distance between sidebands as a function of modulation of the 1.3 μm laser for ^{87}Rb. The arrow points to the value of the modulation that corresponds to the overlap of the sidebands and half the hyperfine splitting of the $6S_{1/2}$ level hyperfine splitting.

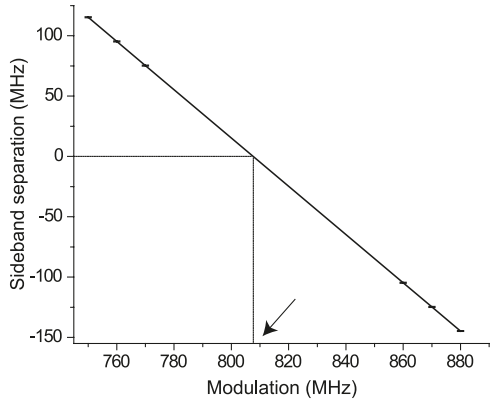

modulation of the 1.3 μm laser. The sidebands that appear on the absorption spectra provide in situ calibration for the energy spacing of the hyperfine splittings. This effectively translates a measurement of energy spacings from the optical region to a much easier measurement in the radio-frequency range.

We observe a rich atomic behavior such as EIT and reversal of the peaks that depend on the power of the lasers, relative polarization, and magnetic-field intensity (see, for example, Fig. 13). This points towards a stringent control on experimental parameters for precision studies of energy separations.

4. Precise measurements

Table 1 shows the values of the magnetic-dipole constants using relativistic MBPT [11] with single double (SD) and single double partial triple (SDpT) wave functions and values extracted from measurements of the hyperfine splitting in other electronic states currently in the literature for $J = 1/2$ [4, 5, 12–14]. We have not been able to find, in the literature, values for higher levels with adequate precision to include them in Table 1. The agreement of theory with the experiment, for

Fig. 13. Absorption spectrum of the 795 nm pump laser as a function of the detuning of the modulated probe. Non desired features appear in the spectrum when the experimental parameters are not under control.

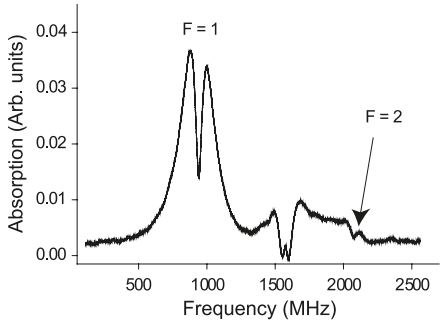

Table 1. Single double (SD) and partial triple (SDpT) excitation calculated from ab initio many-body perturbation theory in ref. 11 and experiment magnetic dipole constants for the first $J = 1/2$ levels in ^{85}Rb. (Adapted from ref. 2).

	SD [MHz]	SDpT [MHz]	Experiment [MHz]
$5S_{1/2}$	642.6	1011.1	1011.910813(2) [12]
$5P_{1/2}$	69.8	120.4	120.499 (10) [13]
$6S_{1/2}$	171.6	238.2	239.18(3) [2, 15]
$6P_{1/2}$	24.55	39.02	39.11(3) [5, 14]
$7S_{1/2}$	70.3	94.3	94.658(19) [4]

$J = 1/2$ levels, is well within the 1% level. The SDpT relativistic wave functions do indeed improve the accuracy of the calculations of the single double wave functions.

The accuracy of the $6S_{1/2}$ measurement is high enough to extract a hyperfine anomaly [15] in an excited state, which shows that the effect is independent of the n state of the level, as originally predicted by Bohr and Weiskopf [16].

5. Conclusions

Two-color modulation transfer spectroscopy has been presented as a reliable and simple method for studying the atomic properties in excited states. The characteristic sidebands appearing the spectra have the two-fold utility of working as an in situ ruler for measurements of energy separations or to lock the frequency of a laser to an excited transition. The good quality of the data presented is due to monitoring the absorption of the pump beam instead of direct absorption of the probe beam. The absorption of the pump beam (or lack thereof) is always guaranteed since a vast number of atoms are always in the ground state and even small changes, i.e., excitation to the last step of the transition, will be noticeable even for small powers of the pump beam. In addition, the spectra does not show a Doppler background due to the lack of an equilibrium thermal population in the intermediate state. It is to be hoped that the method will stimulate studies of atomic properties of excited states and further push the experimental precision and theoretical work in excited atomic states.

Acknowledgments

Work supported by NSF. A.P.G. would like to thank E. Gomez for discussions on the subject of this article and P. Barberis for help on the theory of three-level atoms.

References

1. W. Demtröder. Laser spectroscopy. Springer-Verlag, New York. 1996.
2. A. Pérez Galván, Y. Zhao, and L.A. Orozco. Phys. Rev. A, **78**, 012502 (2008).
3. W.-K. Lee, H.S. Moon, and H.S. Suh. Opt. Lett. **32**, 2810 (2007).
4. H.-C. Chui, M.-S. Ko, Y.-W. Liu, J.-T. Shy, J.-L. Peng, and H. Ahn. Opt. Lett. **30**, 842 (2005).
5. A. Marian, M.C. Stowe, J.R. Lawall, D. Felinto, and J. Ye. Science, **306**, 2063 (2004).
6. W.R. Johnson. Atomic structure theory: lectures on atomic physics. Springer, New York, NY. 2007.
7. V. Wong, R.S. Bennink, A. Marino, R.W. Boyd, and C.R. Stroud, Jr. Phys. Rev. A, **70**, 053811 (2004).
8. J.E. Simsarian, L.A. Orozco, G.D. Sprouse, and W.Z. Zhao. Phys. Rev. A, **57**, 2448 (1998).
9. E. Gomez, F. Baumer, A. Lange, L.A. Orozco, and G.D. Sprouse. Phys. Rev. A, **72**, 012502 (2005).
10. J. Gea-Banacloche, Y.-Q. Li, S.-Z. Jin, and M. Xiao. Phys. Rev. A, **51**, 576 (1995).
11. M.S. Safronova, W.R. Johnson, and A. Derevianko. Phys. Rev. A, **60**, 4476 (1999).
12. E. Arimondo, M. Inguscio, and P. Violino. Rev. Mod. Phys. **49**, 31 (1977).
13. G.P. Barwood, P. Gill, and W.R.C. Rowley. Appl. Phys. B, **53**, 142 (1991).
14. A. Marian, M.C. Stowe, D. Felinto, and J. Ye. Phys. Rev. Lett. **95**, 023001 (2005).
15. A. Pérez Galván, Y. Zhao, L.A. Orozco, E. Gomez, F.J. Baumer, A.D. Lange, and G.D. Sprouse. Phys. Lett. **655B**, 114 (2007).
16. A. Bohr and V.F. Weisskopf. Phys. Rev. **77**, 94 (1950).